

Higgs plus two jet production via gluon fusion as a signal at the CERN LHC

G. Klämke and D. Zeppenfeld

*Institut für Theoretische Physik, Universität Karlsruhe, P.O.Box 6980, 76128 Karlsruhe,
Germany*

Abstract

Higgs boson production in association with two tagging jets will be mediated by electroweak vector boson fusion and by gluon fusion processes at the CERN LHC. The characteristic distributions for the gluon fusion process are analyzed for the $H \rightarrow W^+W^-$ signal at $m_H = 160$ GeV, with subsequent leptonic decay of the W -pair. The dominant backgrounds from top-quark pair production, $WWjj$ production and vector boson fusion processes can be suppressed to a level of $S/B \approx 1/4$, yielding a highly significant gluon fusion signal with 30 fb^{-1} . Analysis of the azimuthal angle correlations of the two jets provides for a direct measurement of the CP-nature of the Htt Yukawa coupling which is responsible for the effective Hgg vertex.

1 Introduction

Higgs boson production in association with two jets has emerged as a promising channel for Higgs boson discovery [1, 2, 3, 4] and for the study of Higgs boson properties [5, 6] at the CERN Large Hadron Collider (LHC). Interest has concentrated on vector-boson-fusion (VBF), i.e. the weak process $qq \rightarrow qqH$ which is mediated by t channel exchange of a W or Z , with the Higgs boson being radiated off this weak boson. The VBF production cross section measures the strength of the WWH and ZZH couplings, which, at tree level, require a vacuum expectation value for the scalar field. Hence the VBF channel is a sensitive probe of the Higgs mechanism as the source of electroweak symmetry breaking.

Another prominent source of Hjj events are second order real emission corrections to the gluon fusion process. Such corrections were first considered in Ref. [7, 8] in the large top mass limit and have subsequently been evaluated for arbitrary quark masses in the loops which induce the effective coupling of the Higgs boson to gluons [9]. Some representative Feynman graphs are shown in Fig. 1. In the $m_t \rightarrow \infty$ limit, also the NLO QCD corrections have recently been calculated [10].

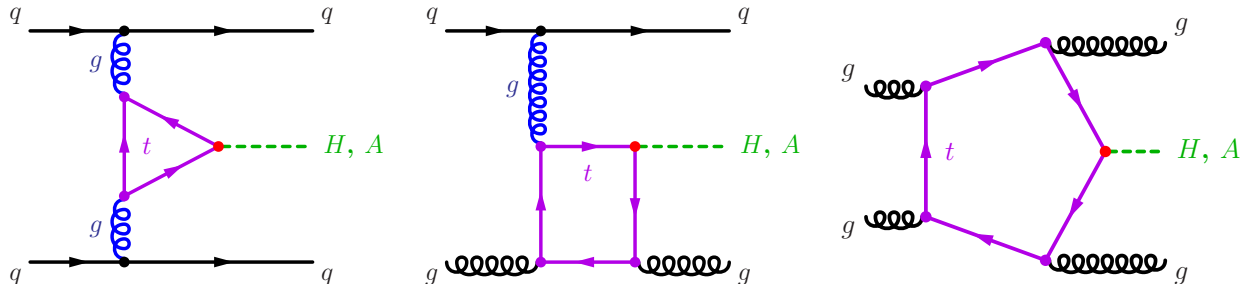


Figure 1: Feynman graphs contributing to $pp \rightarrow Hjj$.

For a SM Higgs boson, the generic Hjj cross section from gluon fusion can somewhat exceed the VBF cross section of a few pb [9]. This raises the question whether gluon fusion induced Hjj events can be used as a source of information for measuring Higgs boson properties. For the VBF process, the most promising Higgs signal arises for Higgs boson masses around W -pair threshold in the channel $pp \rightarrow HjjX$, $H \rightarrow W^+W^- \rightarrow l^+l^- \cancel{p}_T$ [2, 4]. This prompts us to investigate the gluon fusion contribution to this channel for a Higgs boson mass of $m_H = 160$ GeV. We analyze potential background processes, in particular the production of top-quark pairs in association with additional jets, QCD induced $WWjj$ events and VBF processes, and we show in a parton level analysis that the gluon fusion induced Higgs production can be isolated as a highly significant signal with 30 fb^{-1} of LHC data and with a signal to background ratio of about one to four.

The resulting signal is large enough to derive Higgs boson properties from distributions. In this paper we focus on the CP properties of the Yukawa couplings to fermions, which are given by

$$\mathcal{L}_Y = y_f H \bar{\psi}_f \psi_f + i\tilde{y}_f A \bar{\psi}_f \gamma_5 \psi_f, \quad (1)$$

where H and A denote (pseudo)scalar Higgs fields which couple to fermions $f = t, b, \tau$ etc. Via these Yukawa couplings, quark loops induce effective couplings of the Higgs boson to gluons. In our numerical analysis we consider couplings of SM strength, $y_f = \tilde{y}_f = m_f/v = y^{SM}$. In this case the quark loops are dominated by the top quark, and the Higgs gluon coupling can be described by the effective Lagrangian [7, 8]

$$\mathcal{L}_{\text{eff}} = \frac{y_t}{y_t^{SM}} \cdot \frac{\alpha_s}{12\pi v} \cdot H G_{\mu\nu}^a G^{a\mu\nu} + \frac{\tilde{y}_t}{y_t^{SM}} \cdot \frac{\alpha_s}{16\pi v} \cdot A G_{\mu\nu}^a G_{\rho\sigma}^a \varepsilon^{\mu\nu\rho\sigma}, \quad (2)$$

where $G_{\mu\nu}^a$ denotes the gluon field strength. The effective Lagrangian approximation provides an excellent description of the full results for Hjj production, provided one considers modest jet transverse momenta, $p_{Tj} \lesssim m_t$, and Higgs boson masses well below the top quark pair production threshold [9]. We employ the effective Lagrangian description throughout this paper. From the effective Lagrangian emerge Hgg , $Hggg$ and also $Hgggg$ vertices, which correspond to triangle, box and pentagon top quark loops as in Fig. 1.

The structure of the left diagram in Fig. 1 is very similar to the process of Higgs production in vector boson fusion [4]. In Ref. [11] it was shown that the distribution of the azimuthal angle between the two jets in Hjj events can be used to determine the tensor structure of the HVV coupling ($V = W^\pm, Z$). The same method can be applied to Higgs+2 jet production in gluon fusion. Here, the azimuthal angle distribution is sensitive to the tensor structure of the effective Hgg coupling, which is determined by the CP-structure of the top Yukawa coupling. More precisely, neglecting terms which vanish upon contraction with the conserved quark currents, the tensor structure of the Hgg vertex which emerges from Eq.(2) is given by

$$T^{\mu\nu} = a_2 (q_1 \cdot q_2 g^{\mu\nu} - q_1^\nu q_2^\mu) + a_3 \varepsilon^{\mu\nu\rho\sigma} q_{1\rho} q_{2\sigma}, \quad (3)$$

where q_1 and q_2 are the four-momenta of the two gluons. The scalar form factors a_2, a_3 are directly related to the Yukawa interactions of Eq. (1),

$$a_2 = \frac{y_t}{y_t^{SM}} \cdot \frac{\alpha_s}{3\pi v}, \quad a_3 = -\frac{\tilde{y}_t}{y_t^{SM}} \cdot \frac{\alpha_s}{2\pi v} \quad (4)$$

Note that $|a_3| = \frac{3}{2} \cdot |a_2|$ for $y_t = \tilde{y}_t$. Therefore the cross section for the case of a purely CP-odd Yukawa interaction will be about $1.5^2 = 2.25$ times larger than the Standard Model cross section. In contrast to vector boson fusion, there are additional contributions from Higgs plus three and four gluon couplings. These may dilute the sensitivity to the structure of the Hgg vertex and we need to find the regions of phase space with the best analyzing power for differences between CP-even and CP-odd Yukawa couplings.

The paper is organized as follows. In Section 2 we briefly describe the parton level Monte Carlo programs with which we determine the relevant cross sections. All calculations are done at tree level. We then determine the characteristic distributions of the gluon fusion signal and of the various backgrounds in Section 3 and devise cuts which provide a reasonable signal to background ratio and a high statistical signal significance. The measurement of the CP structure of the top Yukawa coupling is addressed in Section 4. We determine the analyzing power of the azimuthal angle correlations between the tagging jets and find that it becomes more pronounced for larger rapidity separations of the jets. Final conclusions are drawn in Section 5.

2 Computational tools

We consider Higgs+2 jet production in gluon fusion (GF) with the Higgs decaying into a pair of W bosons, which, in turn decay leptonically into electrons and muons ($\ell^\pm = e^\pm, \mu^\pm$) and the associated neutrinos: $pp \rightarrow HjjX$, $H \rightarrow W^+W^- \rightarrow \ell^+\ell^-\nu\bar{\nu}$. The dominant backgrounds are from top-pair production, $pp \rightarrow t\bar{t}X$, and from $t\bar{t}$ production with additional jets, $pp \rightarrow t\bar{t}jX$, $pp \rightarrow t\bar{t}jjX$. Another background is W pair production with two accompanying jets, $pp \rightarrow W^+W^-jjX$. This can be a QCD induced process of order $\alpha^2\alpha_s^2$, or it may arise from vector boson fusion, i.e. electroweak processes of the type $qq \rightarrow qqW^+W^-$ at order α^4 . We do not consider backgrounds from Zjj , $Z \rightarrow \tau^+\tau^-$ and from $b\bar{b}jj$ production because they have been shown to be small in the analysis of Ref. [4]. All signal and background cross sections are determined in terms of full tree level matrix elements for the contributing subprocesses and are discussed in more detail below. Detector resolution effects are neglected in the following.

For all our numerical results we simulate pp collisions at a center of mass energy of $\sqrt{s} = 14$ TeV. Standard Model parameters are set to $\sin^2\theta_W = 0.23105$, $M_Z = 91.187$ GeV and $G_F = 1.16637 \cdot 10^{-5}$ GeV $^{-2}$, which translates into $M_W = 79.962$ GeV and $\alpha(M_Z) = 1/128.92$ when using the tree-level relations between these input parameters. For all QCD effects, the running of the strong coupling constant is evaluated at leading order, with $\alpha_s(M_Z) = 0.1298$. We employ CTEQ6L1 parton distribution functions throughout [12].

2.1 The $H + jj$ signal process

The production of a Higgs boson in gluon fusion in association with two jets, at order α_s^4 , can proceed via the subprocesses [7, 8]

$$qq' \rightarrow qq'H, \quad qg \rightarrow qgH, \quad gg \rightarrow ggH, \quad (5)$$

and all crossing related processes. The calculation of this process is based on the work of Ref. [9]. Instead of full top quark loops we express the matrix elements in terms of effective Higgs gluon vertices as given by Eqs. (2,3). We include CP-even and CP-odd Higgs couplings and any interference between them. In addition the program was extended with the matrix elements for the Higgs decay $H \rightarrow W^+W^- \rightarrow \ell^+\ell^-\nu\bar{\nu}$.

Throughout the analysis we use the Standard Model coupling and branching ratio for the Higgs decay into W^+W^- , $B(H \rightarrow W^+W^-) = 0.912$ for a Higgs boson mass of $m_H = 160$ GeV. For the signal process, the factorization scale is chosen as $\mu_f = \sqrt{p_{T_1} \cdot p_{T_2}}$, where $p_{T_{1/2}}$ denote the transverse momenta of the two jets. The strong coupling constant is taken as $\alpha_s^4 = \alpha_s^2(m_H) \cdot \alpha_s(p_{T_1}) \cdot \alpha_s(p_{T_2})$.

2.2 The QCD $t\bar{t} + jets$ backgrounds

Given the Higgs decay signature, the main physics background to the $\ell^\pm\ell^\mp jj\not{p}_T$ signal arises from $t\bar{t} + jets$ production, due to the large production cross section at the LHC and because the branching ratio $B(t \rightarrow Wb)$ is essentially 100%. The basic process we consider is $pp \rightarrow t\bar{t}$, which can be either $gg-$ or $q\bar{q}$ -initiated, with the former strongly dominating at the LHC. Real emission QCD corrections lead to $t\bar{t} + j$ and $t\bar{t} + jj$ events. Relevant subprocesses for the latter are

$$q\bar{q} \rightarrow t\bar{t}g, \quad gg \rightarrow t\bar{t}g, \quad q\bar{q} \rightarrow t\bar{t}q\bar{q}, \quad gg \rightarrow t\bar{t}q\bar{q}, \quad gg \rightarrow t\bar{t}gg \quad (6)$$

and all crossing-related processes [13].

We calculate the $t\bar{t}$, $t\bar{t}j$ and $t\bar{t}jj$ processes at leading order. Hence, for $t\bar{t}+jets$ one has to avoid the phase space regions where the massless jets get soft or collinear with the b quarks, in order to have a finite cross section. In addition, double counting has to be avoided when combining the three background processes. This is achieved in the following way. For the $t\bar{t}jj$ case, we require both tagging jets to arise from massless partons in our simulation. Similarly for $t\bar{t}j$ production, exactly one tagging jet is allowed to arise from a b quark. Finally, the $t\bar{t}$ cross section corresponds to both tagging jets arising from b quarks. With this prescription there is no double counting and the cross sections are finite when applying the cuts described below in Section 3.

The calculation has been performed using the program of Ref. [13]. The decays of the top quarks and W 's are included in the matrix elements, taking into account all off-shell effects for the leptonic final state [14]. In all cases, the factorization scale is chosen as $\mu_f = \min(E_T)$ of the top quarks and additional jets. The overall strong coupling constant factors for the LO $t\bar{t} + n$ jet cross section are calculated as $(\alpha_s)^{n+2} = \prod_{i=1}^{n+2} \alpha_s(E_{T_i})$, where the product runs over n massless partons and the two top quarks.

2.3 The EW $WW + jj$ background

This background arises from W^+W^- bremsstrahlung in quark-(anti)quark scattering via t -channel electroweak boson exchange, with subsequent decay $W^+W^- \rightarrow \ell^+\ell^-\not{p}_T$, i.e.,

$$qq' \rightarrow qq'W^+W^- \rightarrow \ell^+\ell^-\not{p}_T \quad (7)$$

and crossing related processes. The process was calculated with the program VBFNLO [11, 15, 16, 17], which also allows to calculate NLO corrections to distributions. We only use the tree level option, however. In Ref. [17] it was shown that NLO effects are minimized by the factorization scale choice $\mu = Q$ at tree level, where Q is the momentum transfer of the t -channel electroweak boson. With this choice higher order QCD effects are well below 10%. This EW $WW + jj$ background also includes Higgs production in VBF. In fact, for $m_H = 160$ GeV it is dominated by the Higgs contribution, which we here consider as a background to the observation of Hjj production in gluon fusion. In the following we

collectively refer to the VBF Higgs contribution as well as to continuum WW production in VBF as the “EW $WWjj$ ” background.

2.4 The QCD $WW + jj$ background

Real-emission QCD corrections to W^+W^- production give rise to W^+W^-jj events. These background processes include [18]

$$qq' \rightarrow qq'W^+W^-, \quad qg \rightarrow qgW^+W^-, \quad (8)$$

which are dominated by t-channel gluon exchange, and all crossing related processes. The calculation has been done in the framework of the VBFNLO program by employing matrix elements that have been generated with MadGraph [19]. We call these processes collectively the “QCD $WWjj$ ” background. The factorization scale is chosen as $\mu = \min(p_{T_1}, p_{T_2})$ of the two final state partons. The strong coupling constant factor is taken as $\alpha_s^2 = \alpha_s(p_{T_1}) \cdot \alpha_s(p_{T_2})$, i.e. the transverse momentum of each additional parton is taken as the relevant scale for its production.

3 Cross sections at the LHC

The gluon fusion induced $pp \rightarrow HjjX$, $H \rightarrow W^{(*)}W^{(*)} \rightarrow \ell^\pm \ell^\mp \nu \bar{\nu}$ signal is characterized by two high p_T tagging jets and the W decay leptons (e, μ). Here, the tagging jets are defined as the two highest momentum jets in an event. Thus, the signal characteristic is similar to the VBF Higgs signal [4]. However, one cannot simply follow the same search strategy as for VBF. The reason is illustrated in Fig. 2 which shows the rapidity separation, $\Delta\eta_{jj} = |\eta_{j_1} - \eta_{j_2}|$, of the two tagging jets and the dijet invariant mass, m_{jj} , for the signal and the background processes. The three $t\bar{t} + jets$ backgrounds have been combined for clarity, even though their individual distributions are slightly different. The shape of the distributions for $H + jj$ in VBF is very different from that for $H + jj$ in GF which resembles the background distributions. This is because the GF signal shares the characteristics of QCD processes, which are dominated by external gluons. So while these observables are very powerful in the VBF analysis, they are almost useless for separating the GF signal from the background. Therefore, we have to expect a significantly worse signal to background ratio compared to the VBF analyses. In the following we optimize cuts for a Higgs boson mass of $m_H = 160$ GeV. For the calculation of the signal and background processes we impose the following minimal cuts:

$$p_{Tj} > 30 \text{ GeV}, \quad |\eta_j| < 4.5, \quad |\eta_{j_1} - \eta_{j_2}| > 1.0$$

$$p_{T\ell} > 10 \text{ GeV}, \quad |\eta_\ell| < 2.5, \quad \Delta R_{j\ell} = \sqrt{(\eta_j - \eta_\ell)^2 + (\Phi_j - \Phi_\ell)^2} > 0.7 \quad (9)$$

Thus, the jets are required to have a transverse momentum of more than 30 GeV and a rapidity below 4.5 to be detected in the hadronic calorimeter. In the same way the two

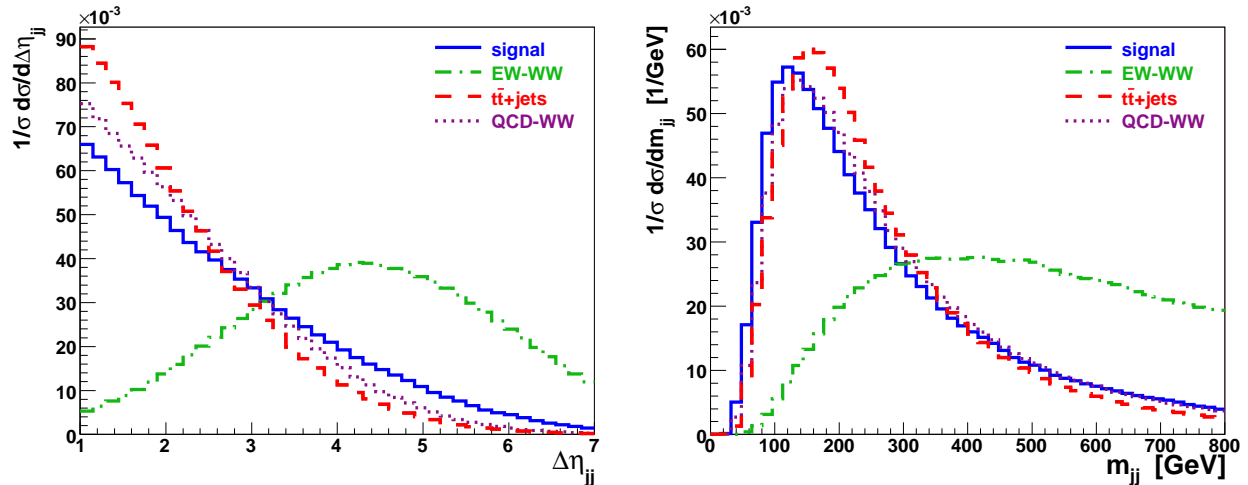


Figure 2: Normalized rapidity separation (*left*) and dijet invariant mass (*right*) distribution of the two tagging jets for the signal (solid) and backgrounds: EW W^+W^-jj (dash-dotted), $t\bar{t} + jets$ (dashed) and QCD W^+W^-jj (dotted). The cuts of Eq. (9) are imposed.

charged leptons are required to have at least 10 GeV of transverse momentum and they should be sufficiently central in order to provide tracking information. Furthermore the jets and leptons are forced to be well separated from each other. Below we will argue for a substantially higher p_T threshold for the charged leptons. Hence, standard LHC lepton triggers will have a very high efficiency for these W -pair events.

At the level of the inclusive cuts of Eq. (9) we require only a modest rapidity separation of $\Delta\eta_{jj} > 1$ for the two tagging jets which are defined as the two highest p_T jets of an event. In contrast to the VBF studies, we do not require the two leptons to lie between these two tagging jets. Instead we will focus on angular and mass cuts of the Higgs decay products to isolate the signal.

The cross sections resulting for the cuts of Eq. (9) are shown in the first line of Table 2. The signal cross section of 115 fb (which includes the branching ratios into leptons) is quite sizeable. The QCD $WWjj$ cross section is about 3 times higher whereas the VBF process reaches 2/3 of the signal rate. The worst source of background arises from the $t\bar{t}$ processes, however, with a combined cross section of about 18 pb.

In order to reduce this large $t\bar{t}$ background it is necessary to make use of a b -veto, that is to discard all events where one or both jets are tagged as b jets. We allow for an overall mistagging probability of 10% for light partons with $p_T > 30$ GeV and $|\eta| < 2.4$, which leads to an acceptable reduction of less than 20% for the signal and all non- $t\bar{t}$ backgrounds. We use the results of the CMS analysis of Ref. [20] for our assumptions on b -veto efficiencies and mistagging probabilities. For a 10% mistagging probability per jet one finds b -veto efficiencies in the range of 60% - 75%, depending on jet transverse momentum and rapidity (p_T, η) as shown in Table 1. With the b -veto, the top backgrounds are reduced by factors of 3 to 8 as shown in line 2 of Table 2. The b -veto is less efficient for the $t\bar{t}jj$ and $t\bar{t}j$ processes than for the $t\bar{t}$ process since, by definition of the tagging jets, the p_T of the b quark becomes

Table 1: The assumed b -tagging efficiencies as a function of jet p_T and rapidity. From Ref. [20]

	$30 \text{ GeV} < p_T < 50 \text{ GeV}$	$p_T > 50 \text{ GeV}$
$1.4 < \eta < 2.4$	60%	70%
$ \eta < 1.4$	65%	75%

smaller the more massless jets are radiated. This is illustrated in the left plot of Fig. 3. The curve for the $t\bar{t}$ process shows the cut at 30 GeV of Eq. 9 because in this case both b -jets are tagging jets. For the $t\bar{t}j$ and $t\bar{t}jj$ processes either one or both b -jets are distinct from the two tagging jets and therefore the p_T distributions continue below 30 GeV.

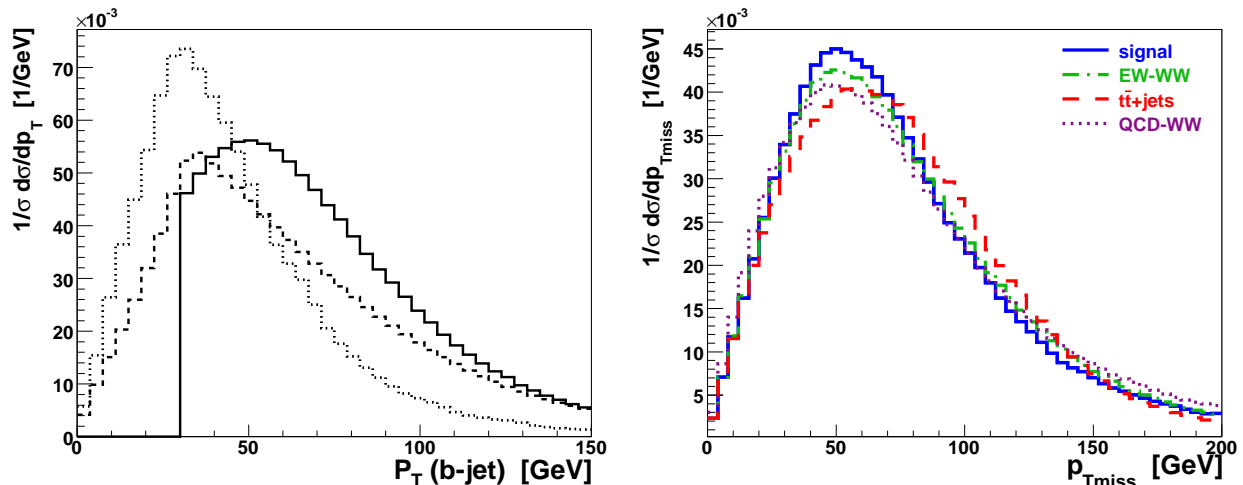


Figure 3: *Left*: Normalized transverse momentum distribution of the b -quarks for $t\bar{t}$ (solid), $t\bar{t}+j$ (dashed) and $t\bar{t}+jj$ (dotted). *Right*: Normalized distribution of the missing transverse momentum for signal and backgrounds as in Fig. 2. The cuts of Eq. (9) are imposed.

A significant difference between signal and background is provided by the angle between the charged decay leptons [21]. In the case where the W pair is produced via the Higgs decay, the W spins are anti-correlated, so the leptons are preferentially emitted in the same direction, close to each other. A large fraction of the backgrounds does not have anti-correlated W spins. This difference is demonstrated in Fig. 4 which shows the R-separation $\Delta R_{\ell\ell}$ and the dilepton invariant mass $m_{\ell\ell}$. The invariant mass can be expressed by

$$m_{\ell\ell} = 2E_{\ell_1}E_{\ell_2}(1 - \cos\theta_{\ell\ell}) \quad (10)$$

with $E_{\ell_{1/2}}$ and $\theta_{\ell\ell}$ being the lepton energy and the dilepton opening angle respectively. Hence, a small opening angle also leads to small $m_{\ell\ell}$ values which is the case for the Higgs signal as compared to the backgrounds [22]. In Fig. 4 the distributions for the electroweak W^+W^-jj background is very similar to the signal distributions because the EW W^+W^-jj process is dominated by Higgs production. We exploit these features by imposing the following

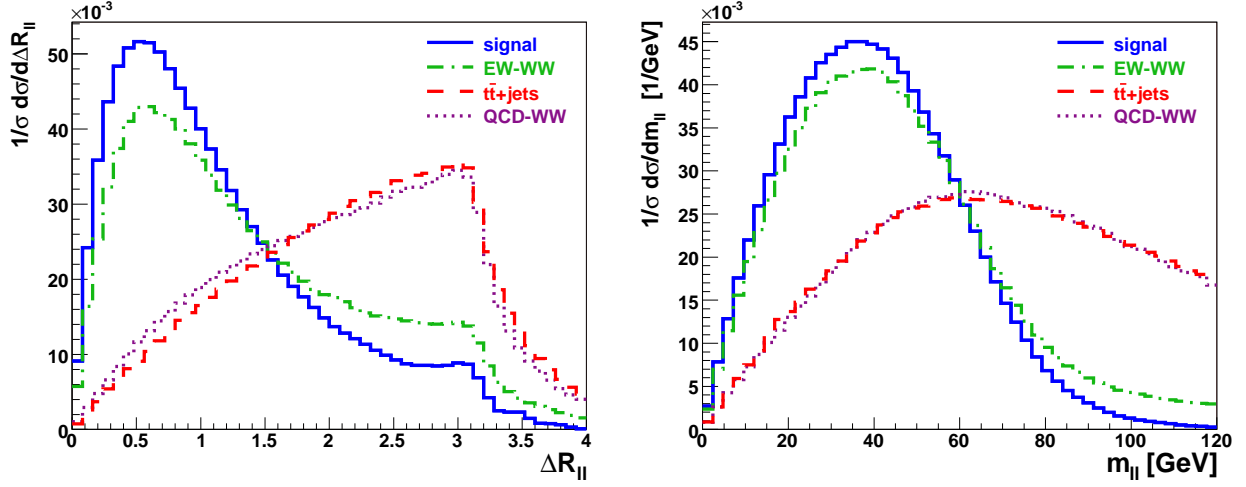


Figure 4: Normalized distributions of the charged leptons R-separation (*left*) and dilepton invariant mass (*right*) after cuts of Eq. (9) for signal and background as in Fig. 2.

lepton-pair angular and mass cuts:

$$\Delta R_{\ell\ell} < 1.1, \quad m_{\ell\ell} < 75 \text{ GeV} \quad (11)$$

The results after these cuts are shown on the third line of Table 2. The signal and the EW W^+W^-jj cross section are cut in half but the other backgrounds are reduced by roughly one order of magnitude.

Table 2: Signal rates for $m_H = 160 \text{ GeV}$ and corresponding background cross sections, in pp collisions at $\sqrt{s} = 14 \text{ TeV}$. Results are given for various levels of cuts and are labeled by equation numbers discussed in the text. All rates are given in fb. The last two columns give the signal to background ratio S/B and the S/\sqrt{B} ratio for an assumed integrated luminosity of 30 fb^{-1} .

cuts	EW						QCD $WWjj$	S/B	S/\sqrt{B}
	GF	$WWjj$	$t\bar{t}$	$t\bar{t}j$	$t\bar{t}jj$	$WWjj$			
inclusive cuts (9)	115.2	75.1	6832	9518	1676	363	1/160	4.6	
+ b veto	99.2	67.4	833	1822	564	307	1/36	9.1	
+ $R_{\ell\ell}, m_{\ell\ell}$ cut (11)	55.8	30.7	104	218	86.4	42.7	1/8.6	13.9	
+ $p_{T\ell}$ cut (12)	41.5	22.3	38.3	87.7	29.2	20.5	1/4.8	16.2	
+ m_T^{WW} cuts (15,16)	37.1	19.9	30.1	63.4	19.3	13.4	1/3.8	16.8	
+ \cancel{p}_T cut (17)	31.5	16.5	23.3	51.1	11.2	11.4	1/3.6	16.2	

Examining the lepton p_T distributions, it turns out that background events which survive the angular cut of Eq. (11) have a significantly lower lepton p_T than the signal and VBF events. This is demonstrated in Fig. 5: On the left hand side the distributions of minimum

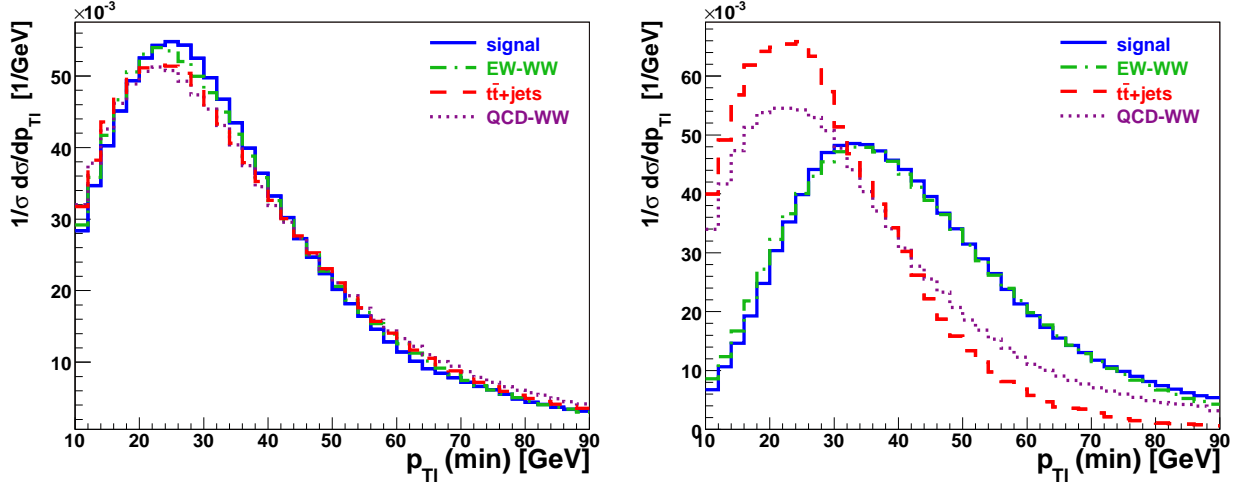


Figure 5: Normalized distributions of the minimum charged lepton p_T for inclusive cuts of Eq. (9) (*left*) and after the additional $\Delta R_{\ell\ell}$ and $m_{\ell\ell}$ cuts of Eq. (11) (*right*). Curves are for signal and backgrounds as in Fig. 2.

lepton p_T are plotted for signal and background, for the inclusive cuts Eq. (9). The curves lie almost on top of each other and there seems to be no difference between the various processes. The right hand side of Fig. 5 shows the same distributions after applying the $R_{\ell\ell}$ and $m_{\ell\ell}$ cut. This suggests a harder lepton p_T cut and we impose

$$P_{T\ell} > 30 \text{ GeV} \quad (12)$$

in the following. Note that this harder cut on the two charged leptons implies excellent trigger efficiencies even in high luminosity running.

It is known that the transverse mass of the dilepton- \cancel{p}_T system can be used to reconstruct the Higgs boson mass. This works particularly well for masses at or below W pair threshold. We here use the transverse mass definition of Ref. [4],

$$m_T^{WW} = \sqrt{(\cancel{E}_T + E_{T,\ell\ell})^2 - (\vec{p}_{T,\ell\ell} + \vec{\cancel{p}}_T)^2} \quad (13)$$

in terms of the invariant mass of the two charged lepton and the transverse energies

$$E_{T,\ell\ell} = (p_{T,\ell\ell}^2 + m_{\ell\ell}^2)^{1/2}, \quad \cancel{E}_T = (\cancel{p}_T^2 + m_{\ell\ell}^2)^{1/2}. \quad (14)$$

In Fig. 6 the GF signal and the VBF process show a pronounced Jacobian peak in the m_T^{WW} distribution whereas the $t\bar{t} + jets$ and QCD W^+W^-jj backgrounds events are broadly distributed. Since the process of gluon induced Higgs+2 jet production will not be a discovery channel for the Higgs boson, we can assume that the Higgs boson mass is known and we can further optimize our cuts for this mass. Hence we impose a strict cut on the m_T^{WW} observable:

$$m_T^{WW} < 170 \text{ GeV} \quad (15)$$

Considering Eqs. (13) and (14), m_T^{WW} and $m_{\ell\ell}$ are apparently correlated with each other. We find that the ratio $m_{\ell\ell}/m_T^{WW}$ contains further useful information. We apply a cut of the

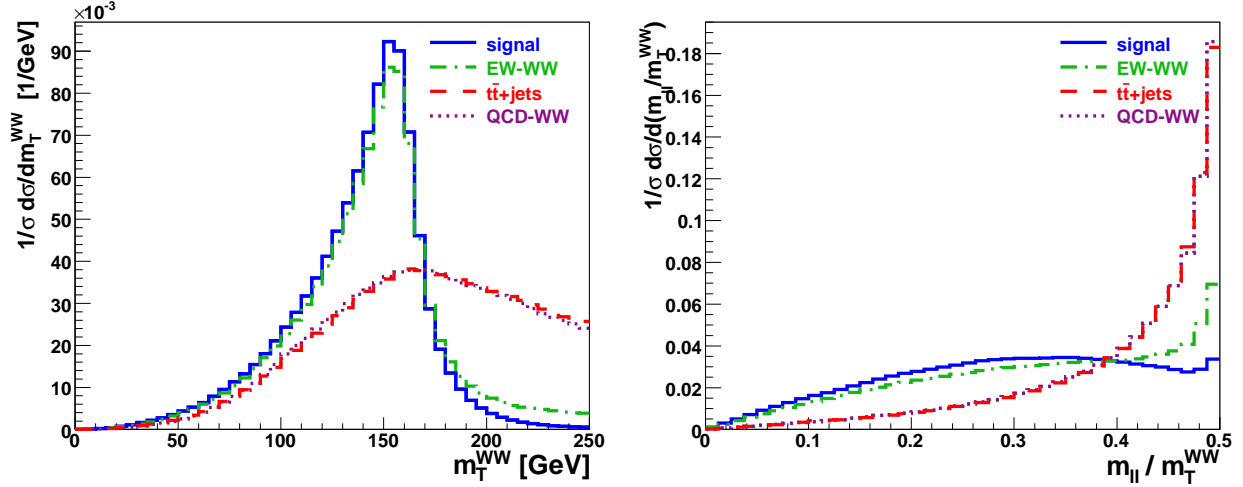


Figure 6: *Left*: Normalized distribution of the transverse mass of the dilepton system as defined in Eq. (13). *Right*: The ratio of the dilepton invariant mass $m_{\ell\ell}$ and transverse mass m_T^{WW} . Curves are for signal and backgrounds as in Fig. 2 with the inclusive cuts of Eq. (9).

form:

$$m_{\ell\ell} < 0.44 \cdot m_T^{WW} \quad (16)$$

With these cuts the backgrounds are again strongly reduced while the Higgs induced processes are affected at the 10% level only. The results for the cuts of Eqs. (12), (15) and (16) are shown in line 4 and 5 of Table 2.

Table 3: Signal and background cross sections and the expected number of events for $\mathcal{L}_{int} = 30 \text{ fb}^{-1}$ at different levels of cuts.

process	inclusive cuts	selection cuts		selection cuts + Eq. (21)	
	σ [fb]	σ [fb]	events / 30 fb^{-1}	σ [fb]	events / 30 fb^{-1}
GF $pp \rightarrow H + jj$	115	31.5	945	10.6	318
EW $pp \rightarrow W^+W^- + jj$	75	16.5	495	13.9	417
$pp \rightarrow t\bar{t}$	6830	23.3	699	1.5	45
$pp \rightarrow t\bar{t} + j$	9520	51.1	1530	13.4	402
$pp \rightarrow t\bar{t} + jj$	1680	11.2	336	3.8	114
QCD $pp \rightarrow W^+W^- + jj$	363	11.4	342	3.0	90
sum of backgrounds	18500	114	3410	35.6	1070

At this level the signal rate is reduced by a factor of 3 as compared to the inclusive cuts, but the backgrounds now have cross sections of the same order as the signal. The largest background still arises from the $t\bar{t}$ processes, especially $t\bar{t} + 1j$, i.e. one tagging jet arises from an (unidentified) b -quark from t or \bar{t} decay and the other one is due to emission of a light quark or gluon in $t\bar{t}$ production. For an integrated luminosity of $\mathcal{L}_{int} = 30 \text{ fb}^{-1}$ the rates correspond

to a purely statistical significance of the gluon fusion signal of $S/\sqrt{B} \approx 17$. However, additional backgrounds arise from $\ell\ell jj$ events where the missing transverse momentum is generated by detector effects. It has been shown in Ref. [4] that these backgrounds are under control when requiring a missing p_T of at least 30 GeV:

$$\cancel{p}_T > 30 \text{ GeV} \quad (17)$$

The \cancel{p}_T distributions are shown on the right hand side of Fig. 3. The GF signal and the backgrounds which we have considered are affected similarly by this cut. The resulting cross sections are shown in the last line of Table 2. We are left with a signal to background ratio of one over 3.6. For $\mathcal{L}_{int} = 30 \text{ fb}^{-1}$ we expect 945 signal events on top of 3400 background events as summarized in Table 3. This corresponds to a statistical significance of $S/\sqrt{B} \approx 16$. Note, however, that the top-production backgrounds need to be understood with an accuracy of 7% or better in the signal region in order to allow for a 5σ Higgs signal from rate measurements alone. If background uncertainties turn out to be that large one may want to reexamine the selection. A significantly higher signal to background ratio, and a concomitant smaller effect of background uncertainties, can be achieved by more aggressive cuts, as is obvious from the various distributions in Figs. 4 to 7. In the absence of solid estimates for systematic errors we have tried to optimize the statistical significance and leave further refinements to future studies. In any case, the event rates summarized in Table 3 are sufficiently large to allow the analysis of distributions.

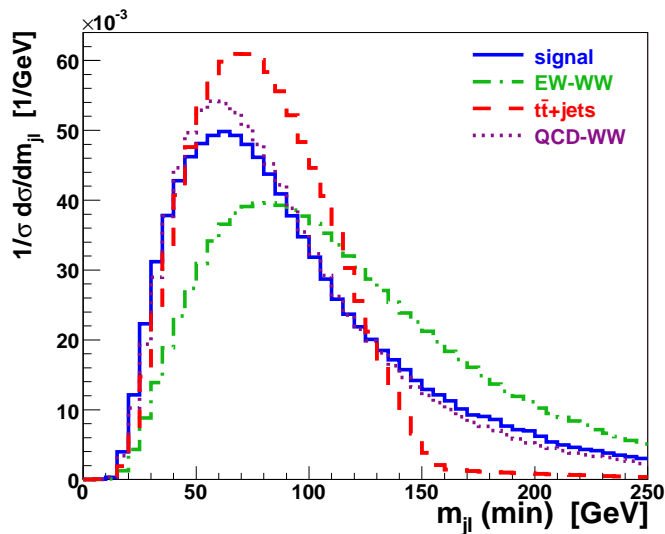


Figure 7: Normalized distributions for the minimum jet-lepton invariant mass. Curves are for signal and backgrounds as in Fig. 2 with the inclusive cuts of Eq. (9).

It is clear that a cut based analysis as described above is not the optimal way to isolate the signal from the background. More advanced techniques like neural networks or likelihood methods should be considered. As input for such refinements we show one further observable, which, however, could not be exploited in our cut based approach. The minimum jet-lepton transverse mass m_{jl} , i.e. the minimum of the four combinations of the charged leptons with the two tagging jets, is plotted in Fig. 7. The distribution shows that m_{jl} is bounded by the

top mass for the $t\bar{t}$ processes. Only a small tail is left above m_t for the $t\bar{t}jj$ process. This characteristic remains after the selection cuts. Since the contribution from top backgrounds is so different for $m_{j\bar{l}} \lesssim 150$ GeV and $m_{j\bar{l}} \gtrsim 150$ GeV, it might be useful to perform separate cut optimizations for the two regions.

4 Azimuthal angle correlations

In order to determine the tensor structure of the effective Hgg coupling, the distributions of the two tagging jets are an important tool. The distribution $d\sigma/d|\Delta\Phi_{jj}|$ of the azimuthal angle between the two tagging jets provides for an excellent distinction between the two tensor structures of Eq. (3) [6]. Unfortunately, when both CP-even and CP-odd couplings of similar strength are present, the tensor structure cannot be unambiguously determined anymore. The missing information is contained in the sign of the azimuthal angle between the tagging jets [11]. Naively one might assume that this sign cannot be defined unambiguously in pp collisions because an azimuthal angle switches sign when viewed along the opposite beam direction. However, in doing so, the “toward” and the “away” tagging jets also switch place, i.e. one should take into account the correlation of the tagging jets with the two distinct beam directions. Defining $\Delta\Phi_{jj}$ as the azimuthal angle of the “away” jet minus the azimuthal angle of the “toward” jet, a switch of the two beam directions leaves the sign of $\Delta\Phi_{jj}$ intact. To be precise, let us define the normalized four-momenta of the two proton

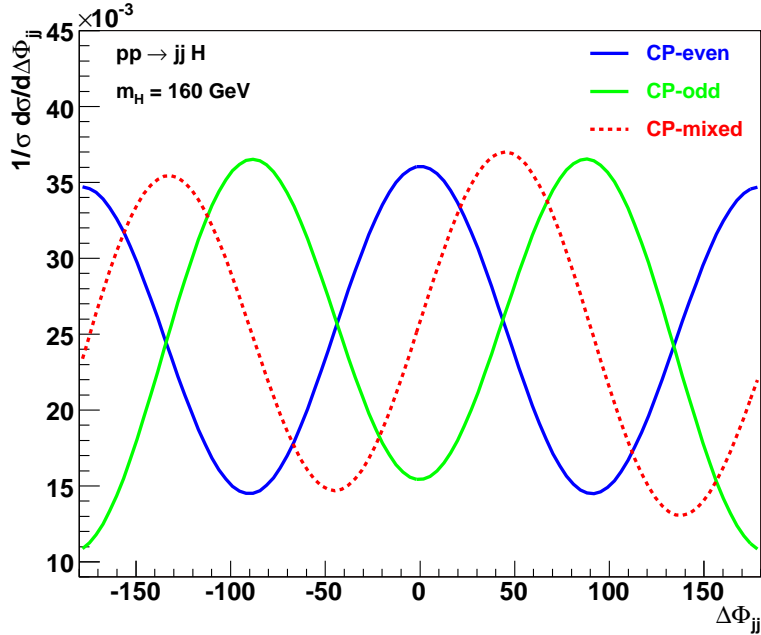


Figure 8: Normalized distributions of the jet-jet azimuthal angle difference as defined in Eq. (18). The curves are for the SM CP-even case ($a_3 = 0$), a pure CP-odd ($a_2 = 0$) and a CP-mixed case ($a_2 = a_3 \neq 0$). The cuts of Eq. (9) and (21) were applied.

beams as b_+ and b_- , while p_+ and p_- denote the four momenta of the two tagging jets, where p_+ points into the same detector hemisphere as b_+ . Then

$$\varepsilon_{\mu\nu\rho\sigma} b_+^\mu p_+^\nu b_-^\rho p_-^\sigma = 2p_{T,+} p_{T,-} \sin(\phi_+ - \phi_-) = 2p_{T,+} p_{T,-} \sin \Delta\Phi_{jj} \quad (18)$$

provides the sign of $\Delta\Phi_{jj}$. This definition is manifestly invariant under the interchange $(b_+, p_+) \leftrightarrow (b_-, p_-)$, i.e. when viewing the event from the opposite beam direction, and we also note that $\Delta\Phi_{jj}$ is a parity odd observable.

The corresponding azimuthal angle distribution is shown in Fig. 8 for the gluon fusion Higgs signal for three scenarios of CP-even and CP-odd Higgs couplings. All three cases are well distinguishable. The maxima in the distribution are directly connected to the size of the parameters a_2 and a_3 , which were introduced in Eqs. (3,4). For

$$a_2 = a \cos \alpha, \quad a_3 = a \sin \alpha, \quad (19)$$

the positions of the maxima are at $\Delta\Phi_{jj} = \alpha$ and $\Delta\Phi_{jj} = \alpha \pm \pi$. This also explains why $|\Delta\Phi_{jj}|$ loses information in the mixed CP case: when folding over the $\Delta\Phi_{jj}$ -distribution at $\Delta\Phi_{jj} = 0$, maxima and minima at $+45$ and -45 degrees cancel each other.

As noted above, $\Delta\Phi_{jj}$ is a parity odd observable. Finding a $\Delta\Phi_{jj}$ asymmetry as in Fig. 8 would show that parity is violated in the process $pp \rightarrow HjjX$. Since the QCD couplings are parity conserving, the parity violation must originate from a parity-odd Higgs coupling, namely a_3 in the effective Hgg vertex. This term is also CP-odd. Such a coupling, occurring at the same time as the CP-even SM coupling a_2 , implies CP-violation in the Higgs sector. In this sense, the observation of an asymmetry in the $\Delta\Phi_{jj}$ distribution would directly demonstrate CP-violation in the Higgs sector.

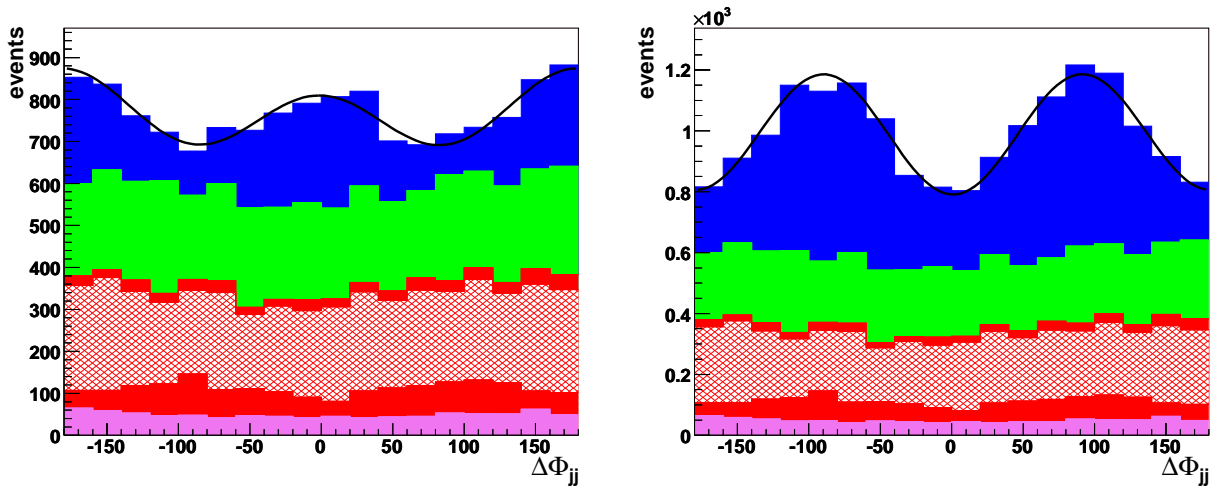


Figure 9: The $\Delta\Phi_{jj}$ distribution for a pure CP-even coupling (*left*) and a pure CP-odd coupling (*right*) for $\mathcal{L}_{int} = 300 \text{ fb}^{-1}$. From top to bottom: GF signal, EW W^+W^-jj , $t\bar{t}$, $t\bar{t}j$, and QCD W^+W^-jj backgrounds.

The azimuthal angle difference $\Delta\Phi_{jj}$ of the two tagging jets is the observable that carries information about the CP nature of the Htt coupling. After we have improved the S/\sqrt{B}

ratio as much as possible by means of selection cuts, we now want to extract this information from the $\Delta\Phi_{jj}$ distribution. For this purpose we define a fit function

$$f(\Delta\Phi) = N(1 + A \cos[2(\Delta\Phi - \Delta\Phi_{max})] - B \cos(\Delta\Phi)), \quad (20)$$

with fit-parameters $A, \Delta\Phi_{max}, B, N$. The parameter N is a normalization factor and B is an overall shape-factor. The parameters A and $\Delta\Phi_{max}$ are the physically relevant ones. A describes the relative magnitude of the angle correlation and thus the significance of this measurement with respect to the background fluctuations. $\Delta\Phi_{max}$ gives the position of the first maximum, which measures the relative strength of CP-even and CP-odd couplings.

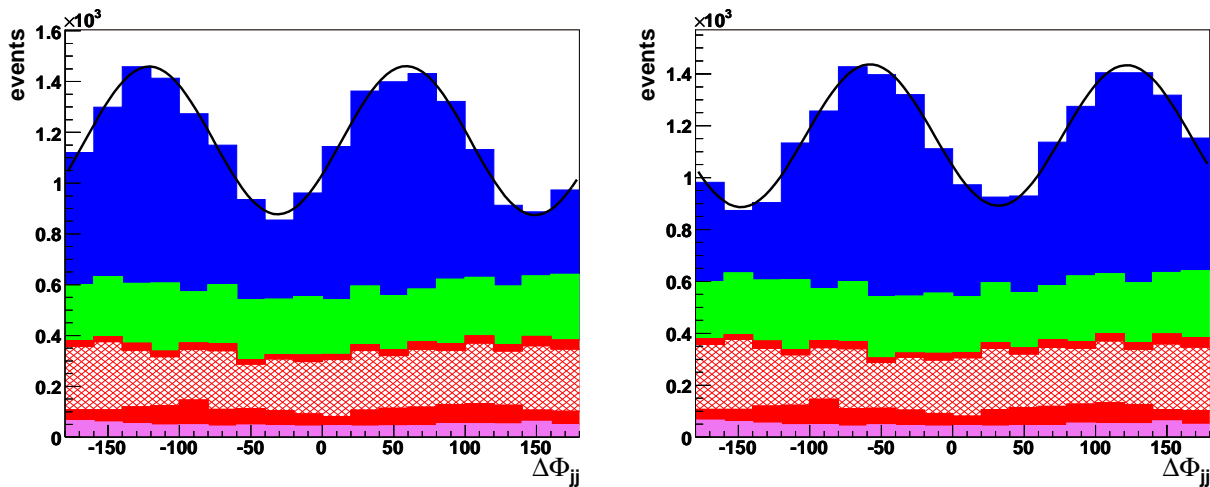


Figure 10: The $\Delta\Phi_{jj}$ distribution for CP-mixed couplings as in Fig. 9 for $\mathcal{L}_{int} = 300 \text{ fb}^{-1}$. *Left:* $y_t = \tilde{y}_t = y_t^{SM}$. *Right:* $y_t = -\tilde{y}_t = y_t^{SM}$.

Figure 9 shows the expected $\Delta\Phi_{jj}$ distribution for a purely CP-even ($y_t = y_t^{SM}$, $\tilde{y}_t = 0$) and a purely CP-odd Htt coupling ($y_t = 0$, $\tilde{y}_t = y_t^{SM}$) for an integrated luminosity of 300 fb^{-1} . Plotted are signal events on top of the various backgrounds. The black curve is the fit to this distribution with the function of Eq. (20). A comparison with Fig. 8 shows that the relevant characteristic angular correlation is kept but diluted due to the background. However with the help of the fit we can extract the parameters A and $\Delta\Phi_{max}$. In order to estimate the statistical significance of the measurement, we divide our Monte Carlo sample into 10 independent samples of data, each corresponding to an integrated luminosity of 30 fb^{-1} . Averaging the results and the errors, we obtain $A = 0.115 \pm 0.039$, $\Delta\Phi_{max} = -3.0 \pm 10.7$ for the CP-even coupling and $A = 0.210 \pm 0.034$, $\Delta\Phi_{max} = 90.4 \pm 4.7$ for the CP-odd coupling, where errors are purely statistical. The expected values would be $\Delta\Phi_{max} = 0$ and $\Delta\Phi_{max} = 90$ respectively. Since the difference between the CP-even and the CP-odd case can also be expressed as a flip in the sign of A (keeping $\Delta\Phi_{max} = 0$) this result means that a CP-odd Htt coupling can be distinguished from the SM case with approximately 6σ significance for 30 fb^{-1} , assuming a perfect detector. Since the backgrounds are fairly flat in $\Delta\Phi_{jj}$, any background normalization uncertainties are largely absorbed into the fit parameters N and B . Our estimates for the significance of the A determination will therefore receive minor changes due to such systematic errors.

Fig. 10 shows the the azimuthal angle distribution for the case of a CP-mixed coupling $y_t = \pm \tilde{y}_t = y_t^{SM}$. Applying the method described above, we extract $A = 0.260 \pm 0.031$, $\Delta\Phi_{max} = 59.3 \pm 3.5$ from the left part of Fig. 10 and $A = 0.246 \pm 0.031$, $\Delta\Phi_{max} = -58.4 \pm 3.7$ from the right one. The expected values would be $\Delta\Phi_{max} = \pm \arctan(\frac{3}{2}) = \pm 56.3$.

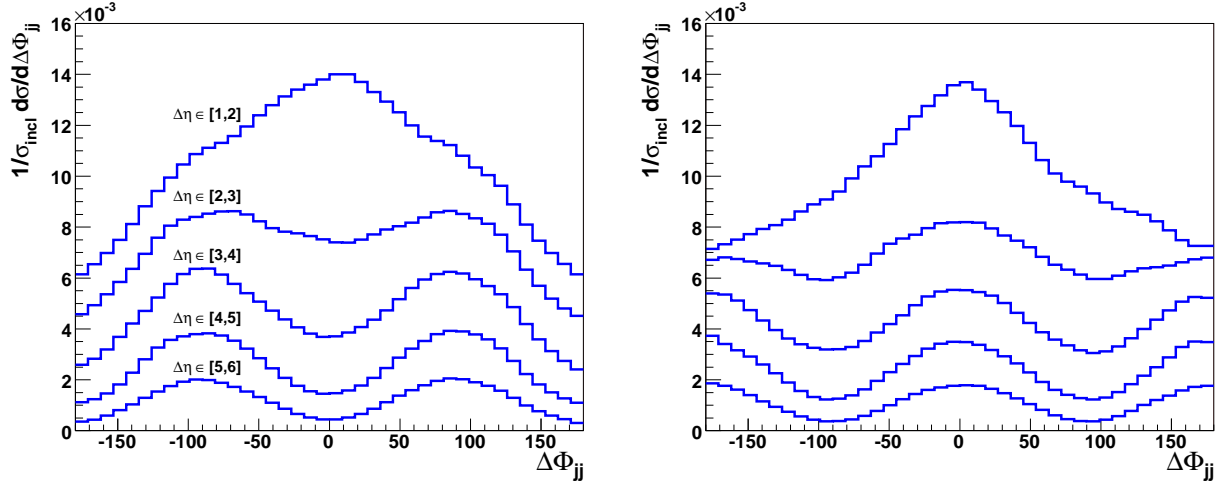


Figure 11: The $\Delta\Phi_{jj}$ distribution of the signal for different intervals of the jet rapidity separation $\Delta\eta_{jj}$ as labeled in the left plot. *Left*: CP-even coupling. *Right*: CP-odd coupling.

For the procedure described above, we have applied an additional cut on the dijet rapidity separation of

$$\Delta\eta_{jj} = |\eta_{j1} - \eta_{j2}| > 3.0 \quad (21)$$

This is advantageous because the analyzing power of the $\Delta\Phi_{jj}$ distribution strongly depends on the rapidity separation of the two tagging jets. This is demonstrated in Fig. 11 which shows the distributions within different $\Delta\eta_{jj}$ intervals for the CP-even and the CP-odd case. For low $\Delta\eta_{jj}$ values the $\Delta\Phi_{jj}$ distribution does not show the characteristic features discussed above. However, they get more pronounced as $\Delta\eta_{jj}$ increases. Therefore, a cut on $\Delta\eta_{jj}$ raises the analyzing power of the azimuthal angle distribution. Unfortunately, an additional cut also decreases the number of signal events and thus the significance of the measurement. It turns out that a cut value around $\Delta\eta_{cut} \approx 3$ leads to a minimal error on $\Delta\Phi_{max}$ and an optimal $\Delta A/A$ ratio.

Our analysis has been performed with parton level Monte Carlo programs based on leading order matrix elements for the signal and the backgrounds. In the similar situation of widely separated dijets in $p\bar{p}$ collisions at the Tevatron, some de-correlation in the azimuthal angle distribution is predicted at higher order at the parton level [23, 24, 25, 26, 27] and with parton showers and hadronisation [28, 29], and measured at the Tevatron [30]. A strong de-correlation, as originally predicted in a pure parton shower approach in Ref. [31], would invalidate our method for Higgs CP studies. Using full leading order QCD matrix elements for $H + 2$ - and $H + 3$ -parton production and additional parton shower simulation, the question was reanalyzed recently [32] and a de-correlation at the 25% level was found for rapidity separations $\Delta\eta_{jj} > 4.2$, which would imply a corresponding reduction of A in

Eq. (20). An even smaller effect was found in the NLO calculation of Campbell et al. [10], raising the possibility that part of the de-correlation found in Ref. [32] is due to tagging jets originating from the parton shower, which is generated flat in azimuthal angle. Considering these effects we expect a reduction of 25% or less in analyzing power due to higher order effects. A quantitative determination of the de-correlation requires further study, however.

5 Conclusions

Both sources of Higgs plus dijet events at the LHC, vector boson fusion and gluon fusion, can provide important information on Higgs boson properties. Vector boson fusion is sensitive to the couplings of the Higgs boson to weak bosons, gluon fusion measures the effective Hgg coupling, which, within the SM, is mostly induced by the Htt Yukawa coupling. For a Higgs boson mass of 160 GeV and SM couplings, the decay channel $H \rightarrow WW \rightarrow l^+l^- \cancel{p}_T$ provides a highly significant signal for both the vector boson fusion [4] and the gluon fusion signal above backgrounds, which are dominated by top quark pair production. The distinction of the two Hjj channels is most easily achieved, at the statistical level, by using characteristically different distributions of the two tagging jets, mainly their rapidity separation and the dijet invariant mass [33]. A central jet veto can be used to further enhance vector boson fusion over gluon fusion events [4].

A further analysis of the structure of the Htt Yukawa coupling, in particular the question whether this coupling is CP-even or CP-odd or a mixture of the two, is possible via the azimuthal angle correlation of the two tagging jets. Taking into account the rapidity correlations of the tagging jets with the beam directions, the sign of this azimuthal angle can be defined [11] and the resulting full distribution in azimuthal angle separation $\Delta\Phi_{jj}$ exhibits the relative strength of CP-even and CP-odd couplings via a phase shift. The $\Delta\Phi_{jj}$ distribution is sensitive to CP violation in the Higgs sector. For the case analyzed here, $m_H = 160$ GeV with SM size production cross section in gluon fusion and SM-like decay branching fractions, a highly significant measurement is expected with an integrated luminosity well below 100 fb^{-1} . A precise determination of the analyzing power requires a full detector simulation, however, which is beyond the scope of the present paper.

The methods presented here for the particular case of $m_H = 160$ GeV, can be extended to other Higgs boson masses. For $150 \text{ GeV} \lesssim m_H \lesssim 2m_Z$ the present analysis should be readily applicable, with minor modifications, like in the transverse mass cut of Eq. (15). Lower Higgs boson masses may require somewhat softer lepton p_T cuts and will eventually run into statistical problems due to the smaller branching ratio for $H \rightarrow WW$ decay as compared to $m_H = 160$ GeV. The azimuthal angle correlations of the tagging jets are independent of the specific Higgs decay mode, of course. This raises the question whether $H \rightarrow \tau\tau$ or $H \rightarrow \gamma\gamma$ signals from gluon fusion induced Hjj events are observable at the LHC. Given the much more difficult task of QCD background reduction as compared to vector boson fusion studies which we have found in this paper for the “easy” $m_H = 160$ GeV case, we expect such novel Higgs signals from gluon fusion induced Hjj events and the study of their azimuthal angle

correlations to be quite challenging, but worth considering.

6 Acknowledgments

We are grateful to Barbara Jäger, Vera Hankele, Manuel Bähr and Michael Kubocz for many useful discussions. This research was supported in part by the Deutsche Forschungsgemeinschaft under SFB TR-9 “Computational Particle Physics”. G. K. gratefully acknowledges DFG support through the Graduiertenkolleg “High Energy Physics and Particle Astrophysics”.

References

- [1] ATLAS Collaboration, ATLAS TDR, Report No. CERN/LHCC/99-15 (1999); E. Richter-Was and M. Sapinski, *Acta Phys. Pol. B* **30**, 1001 (1999);
- [2] S. Asai *et al.*, *Eur. Phys. J. C* **32S2**, 19 (2004) [arXiv:hep-ph/0402254].
- [3] G. L. Bayatian *et al.*, CMS TDR, Report No. CERN/LHCC/2006-021 (2006); R. Kinnunen and D. Denegri, CMS Note No. 1997/057; R. Kinnunen and A. Nikitenko, Report No. CMS TN/97-106; R. Kinnunen and D. Denegri, arXiv:hep-ph/9907291.
- [4] D. L. Rainwater, PhD thesis, arXiv:hep-ph/9908378; D. Rainwater and D. Zeppenfeld, *Phys. Rev. D* **60**, 113004 (1999) [Erratum-ibid. *D* **61**, 099901 (2000)] [arXiv:hep-ph/9906218]; N. Kauer, T. Plehn, D. Rainwater, and D. Zeppenfeld, *Phys. Lett. B* **503**, 113 (2001) [arXiv:hep-ph/0012351].
- [5] D. Zeppenfeld, R. Kinnunen, A. Nikitenko, and E. Richter-Was, *Phys. Rev. D* **62**, 013009 (2000) [arXiv:hep-ph/0002036]; D. Zeppenfeld, in *Proc. of the APS/DPF/DPB Summer Study on the Future of Particle Physics, Snowmass, 2001* edited by N. Graf, eConf **C010630**, p. 123 (2001) [arXiv:hep-ph/0203123]; A. Belyaev and L. Reina, *JHEP* **0208**, 041 (2002) [arXiv:hep-ph/0205270]; M. Dührssen *et al.*, *Phys. Rev. D* **70**, 113009 (2004) [arXiv:hep-ph/0406323].
- [6] T. Plehn, D. Rainwater, and D. Zeppenfeld, *Phys. Rev. Lett.* **88**, 0518011 (2002); V. Hankele, G. Klämke, and D. Zeppenfeld, arXiv:hep-ph/0605117;
- [7] R. P. Kauffman, S. V. Desai and D. Risal, *Phys. Rev. D* **55** (1997) 4005 [Erratum-ibid. *D* **58** (1998) 119901] [arXiv:hep-ph/9610541].
- [8] R. P. Kauffman and S. V. Desai, *Phys. Rev. D* **59** (1999) 057504 [arXiv:hep-ph/9808286].
- [9] V. Del Duca, W. Kilgore, C. Oleari, C. Schmidt and D. Zeppenfeld, *Phys. Rev. Lett.* **87** (2001) 122001 [arXiv:hep-ph/0105129] and *Nucl. Phys. B* **616** (2001) 367 [arXiv:hep-ph/0108030].

- [10] R. K. Ellis, W. T. Giele and G. Zanderighi, Phys. Rev. D **72**, 054018 (2005) [Erratum-ibid. D **74**, 079902 (2006)] [arXiv:hep-ph/0506196]; R. K. Ellis, W. T. Giele and G. Zanderighi, Phys. Rev. D **73**, 014027 (2006) [arXiv:hep-ph/0508308]; J. M. Campbell, R. Keith Ellis and G. Zanderighi, JHEP **0610** (2006) 028 [arXiv:hep-ph/0608194].
- [11] V. Hankele, G. Klämke, D. Zeppenfeld and T. Figy, Phys. Rev. D **74** (2006) 095001 [arXiv:hep-ph/0609075].
- [12] J. Pumplin, D. R. Stump, J. Huston, H. L. Lai, P. Nadolsky and W. K. Tung, JHEP **0207**, 012 (2002) [arXiv:hep-ph/0201195].
- [13] N. Kauer, Phys. Rev. D **67** (2003) 054013 [arXiv:hep-ph/0212091].
- [14] N. Kauer and D. Zeppenfeld, Phys. Rev. D **65** (2002) 014021 [arXiv:hep-ph/0107181].
- [15] T. Figy, C. Oleari and D. Zeppenfeld, Phys. Rev. D **68** (2003) 073005 [arXiv:hep-ph/0306109].
- [16] C. Oleari and D. Zeppenfeld, Phys. Rev. D **69** (2004) 093004 [arXiv:hep-ph/0310156].
- [17] B. Jäger, C. Oleari and D. Zeppenfeld, Phys. Rev. D **73** (2006) 113006 [arXiv:hep-ph/0604200].
- [18] V. D. Barger, T. Han, J. Ohnemus and D. Zeppenfeld, Phys. Rev. D **41** (1990) 2782.
- [19] F. Maltoni and T. Stelzer, JHEP **0302** (2003) 027 [arXiv:hep-ph/0208156].
- [20] C. Weiser, CERN-CMS-NOTE-2006-014
- [21] M. Dittmar and H. K. Dreiner, Phys. Rev. D **55**, 167 (1997) [arXiv:hep-ph/9608317].
- [22] V. D. Barger, G. Bhattacharya, T. Han and B. A. Kniehl, Phys. Rev. D **43**, 779 (1991).
- [23] V. Del Duca and C. R. Schmidt, Phys. Rev. **D49** (1994) 4510 [arXiv:hep-ph/9311290].
- [24] W. J. Stirling, Nucl. Phys. **B423** (1994) 56 [arXiv:hep-ph/9401266].
- [25] V. Del Duca and C. R. Schmidt, Nucl. Phys. Proc. Suppl. **39BC** (1995) 137 [arXiv:hep-ph/9408239].
- [26] V. Del Duca and C. R. Schmidt, Phys. Rev. **D51** (1995) 2150 [arXiv:hep-ph/9407359].
- [27] L. H. Orr and W. J. Stirling, Phys. Rev. **D56** (1997) 5875 [arXiv:hep-ph/9706529].
- [28] G. Marchesini and B. R. Webber, Nucl. Phys. **B310** (1988) 461.
- [29] G. Marchesini, B. R. Webber, G. Abbiendi, I. G. Knowles, M. H. Seymour and L. Stanco, Comput. Phys. Commun. **67** (1992) 465.
- [30] S. Abachi *et al.* [D0 Collaboration], Phys. Rev. Lett. **77** (1996) 595 [arXiv:hep-ex/9603010].

- [31] K. Odagiri, JHEP **0303** (2003) 009 [arXiv:hep-ph/0212215].
- [32] V. Del Duca *et al.*, JHEP **0610**, 016 (2006) [arXiv:hep-ph/0608158].
- [33] E. L. Berger and J. Campbell, Phys. Rev. D **70**, 073011 (2004) [arXiv:hep-ph/0403194].